Current Optics and Photonics
Vol. 2, No. 3, June 2018, pp. 261-268

ISSN: 2508-7266(Print) / ISSN: 2508-7274(Online)
DOI: https://doi.org/10.3807/COPP.2018.2.3.261

Terahertz Wave Generation via Stimulated Polariton Scattering in $BaTiO_3$ Bulk Crystal with High Parametric Gain

Zhongyang Li*, Bin Yuan, Silei Wang, Mengtao Wang, and Pibin Bing

College of Electric Power, North China University of Water Resources and Electric Power, Zhengzhou 450045, China

(Received February 7, 2018 : revised April 20, 2018 : accepted May 15, 2018)

Stimulated polariton scattering (SPS) from the A_1 transverse optical (TO) modes of $BaTiO_3$ bulk crystal generating a terahertz (THz) wave with the noncollinear phase-matching (NPM) condition is theoretically investigated. To our best knowledge, this is the first report on THz wave generation from $BaTiO_3$ bulk crystal via SPS. Phase-matching (PM) characteristics in the NPM configuration are analyzed. Effective parametric gain lengths for the Stokes and THz waves in the NPM configuration are calculated. The effective parametric gain coefficient and absorption coefficient of the THz wave in $BaTiO_3$ are theoretically simulated. The THz phonon flux densities generated via SPS in $BaTiO_3$ are theoretically calculated by solving the coupled wave equations under the NPM condition. The PM characteristics and THz-wave parametric gain characteristics in $BaTiO_3$ are compared to those in $MgO:LiNbO_3$. The results of the analysis indicate that $BaTiO_3$ is an attractive optical crystal for efficient THz wave generation via SPS.

Keywords : Terahertz wave, Stimulated polariton scattering, $BaTiO_3$
OCIS codes : (190.4410) Nonlinear optics, parametric processes; (190.4223) Nonlinear wave mixing

I. INTRODUCTION

Stimulated polariton scattering (SPS) has proved to be an efficient scheme to generate terahertz (THz) wave [1-7]. A polariton is a coupled quantum between a pump laser and the infrared- and Raman-active transverse optical (TO) modes in a crystal; it behaves like a phonon near the resonant frequency associated with the TO mode, and exhibits photon-like behavior for lower non-resonant frequencies [8]. SPS is composed of second- and third-order nonlinear frequency-conversion processes in which a pump photon stimulates a Stokes photon at the difference frequency between the pump photon and the polariton. At the same time, a THz wave is generated by the parametric process due to the nonlinearity arising from both electronic and vibrational contributions of the crystal. The TO phonon resonances can contribute substantially to the magnitudes of second- and third-order nonlinearities, which are beneficial to THz generation via SPS. A THz wave parametric oscillator (TPO) based on SPS processes exhibits many advantages, such as narrow linewidth, coherence, a wide range of tunability, high-power output, and room-temperature operation [1-5].

Ferroelectric crystals such as $MgO:LiNbO_3$, $LiTaO_3$, $KTiOPO_4$, $RbTiOPO_4$, and $KTiOAsO_4$ are characterized by strong infrared- and Raman-active TO phonon resonances, which are employed to generate a THz wave via SPS [9-13]. Ferroelectric crystals have a wide transmission range, a relatively high second-order nonlinear coefficient, and a high optical damage threshold. However, the quantum conversion efficiency of SPS in the above mentioned ferroelectric crystals is relatively low. The reasons are as follows: First, the wave vectors of the pump, Stokes, and THz waves are noncollinear, which intensively restricts the interaction volume among the three mixing waves. Second, the effective nonlinear optical coefficients involving both second- and third-order nonlinearities are not large enough. Third, the THz absorption coefficients of ferroelectric

*Corresponding author: thzwave@163.com, ORCID 0000-0001-8350-5781
Color versions of one or more of the figures in this paper are available online.

crystals are extremely large, particularly in high THz frequency range.

Similar to the above mentioned ferroelectric crystals, $BaTiO_3$ has infrared- and Raman-active TO phonon modes, which can be employed to generate THz wave via SPS [14]. $BaTiO_3$ with its perovskite structure has five atoms per unit cell and four sets of optical branches. At room temperature it has a tetragonal unit cell with C_{4v} point-group symmetry, and the optical branches are split into three A_1 and four E infrared- and Raman-active TO modes, and one B_1 Raman-active mode [15]. The four E TO modes in the tetragonal phase, with frequencies of 34, 180, 308 and 498 cm^{-1}, are doubly degenerate, having their polarization along the x- and y- axes [16]. The three A_1 TO modes in the tetragonal phase, with frequencies of 178, 260 and 515 cm^{-1}, are polarized along the z- axis [14]. $BaTiO_3$ is an attractive material for the nonlinear optical interaction between optical and THz waves, due to its wide transmission range (0.4~5 μm) [17], a relatively high nonlinear coefficient ($d_{15} = 13.7$ pm/V at 1064 nm) [18], and a high optical damage threshold (83 GW/cm^2 at 596 nm, with 1 picosecond pulsewidth) [19]. It should be noted that $BaTiO_3$ suffers from severe photorefractive effect [20], so in the process of THz generation by SPS we should avoid the photorefractive effect.

In this Letter, we theoretically study SPS from the A_1 TO modes of $BaTiO_3$ bulk crystal with the noncollinear phase-matching (NPM) condition, for the first time. We analyze the phase-matching (PM) characteristics in the NPM configuration. The effective parametric gain length and effective parametric gain coefficient for the THz wave in the NPM configuration are calculated. THz phonon flux densities in $BaTiO_3$ are theoretically simulated by solving coupled wave equations under NPM conditions.

II. THEORETICAL MODEL

A surface-emitted TPO with a NPM configuration comprises a single-resonant optical parametric oscillator with a Fabry-Perot cavity, as shown in Fig. 1. The configuration was first reported by T. Ikari *et al* [2]. The nonlinear optical crystal is a $BaTiO_3$ crystal. The resonant cavity for the Stokes wave consists of two plane-parallel mirrors M_1 and M_2 with high reflectance. The pump wave passes through the cavity at its edges M_1 and M_2, and the Stokes wave propagates along the x axis of the $BaTiO_3$.A THz wave vector perpendicular to the output surface is achieved by setting the pump wave's angle of incidence to the crystal surface. θ is the angle between the vectors of the pump and Stokes waves within the crystal, and φ is the angle between the vectors of the pump and THz waves within the crystal. To take advantage of the largest nonlinear optical coefficient d_{15} of $BaTiO_3$, we consider that the pump, Stokes and THz waves are an o-wave, o-wave and e-wave respectively. The cavity mirrors and

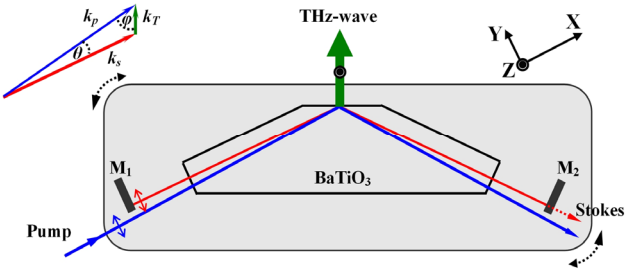

FIG. 1. Schematic diagram of a surface-emitted TPO using $BaTiO_3$ with a NPM configuration. The angle θ is the PM angle between the wave vectors of the pump and Stokes waves, and the angle φ is the PM angle between the wave vectors of the pump and THz waves.

$BaTiO_3$ crystal are mounted on a rotating stage. The wavelengths of the Stokes, and THz waves can be tuned by rotating the stage continuously, since the angle θ changes continuously. Since THz waves are severely absorbed by $BaTiO_3$, it is important to couple the THz wave out of the $BaTiO_3$ before the pump, Stokes and THz waves get absorbed [21].

III. PM CHARACTERISTICS

Coupling of A_1 TO modes and the pump wave creates A_1-symmetry polaritons, with a dispersion curve. Figure 2 shows PM curves for a pump wavelength of 1064 nm, and an A_1-symmetry polariton dispersion curve in $BaTiO_3$. $BaTiO_3$ has a strong A_1 TO mode with a wavenumber of 178 cm^{-1} and two medium-strength A_1 TO modes with wavenumbers of 260 and 515 cm^{-1}. The wavelengths of the Stokes waves generated by SPS depend on the PM angle θ between the pump wave and the Stokes wave, and the

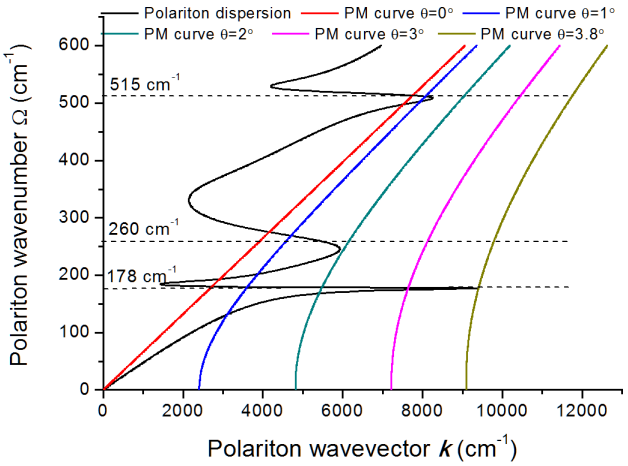

FIG. 2. PM curves with a pump wavelength λ_p of 1064 nm and A_1-symmetry polariton dispersion curve in $BaTiO_3$. $|\boldsymbol{k}| = 2\pi\Omega n_{pol}$, where n_{pol} is the refractive index, and Ω the wavenumber of the polariton.

THz-wave frequencies are determined by the intersections of the PM curves and the A_1-symmetry polariton dispersion curve, as shown in Fig. 2. Polaritons generated by small-angle copropagating interactions between the pump and Stokes waves have terahertz frequencies for the 178 and 260 cm^{-1} TO modes, and far-infrared frequencies associated with the 515 cm^{-1} TO mode. For THz wave generation via SPS, two requirements have to be fulfilled: the energy conservation law $\omega_p = \omega_s + \omega_T$, and the NPM condition $\boldsymbol{k}_p = \boldsymbol{k}_s + \boldsymbol{k}_T$, as shown in the inset of Fig. 1. Here ω_p, ω_s, and ω_T are the angular frequencies and $\boldsymbol{k}_p$, $\boldsymbol{k}_s$, and $\boldsymbol{k}_T$ the wave vectors of the pump, Stokes, and THz wave respectively. The PM condition can be rewritten as $k_T^2 = k_p^2 + k_s^2 - 2k_p k_s \cos\theta$. The theoretical values of the refractive index are calculated using a Sellmeier equation for $BaTiO_3$ in the infrared range [17] and THz range [14]. When the angle θ varies from 0° to 3.8°, the PM curves and the dispersion curve of the A_1-symmetry polariton modes intersect, which means a THz wave can be generated. It should be noted that the PM curve for $\theta = 0°$ intersects the polariton curve in the polariton-resonance region, which indicates that the collinear PM can be realized. At polariton-resonance region the refractive indices and nonlinear susceptibilities vary dramatically. A refractive index of 247 at 5.5 THz in the polariton-resonance region of $KTiOPO_4$ is obtained in backward SPS [7]. In the polariton-resonance region of 178 cm^{-1} in $BaTiO_3$, the refractive indices of THz wave vary dramatically from 1.2 to 8.5. When the refractive index of the THz wave approximately equals those of the pump and Stokes waves, collinear PM can be realized. Owing to the strong coupling between TO mode and pump wave near polariton resonance, nonlinear susceptibilities can be dramatically enhanced, which can be employed to enhance the THz-wave output using a transverse-pumping geometry [22, 23].

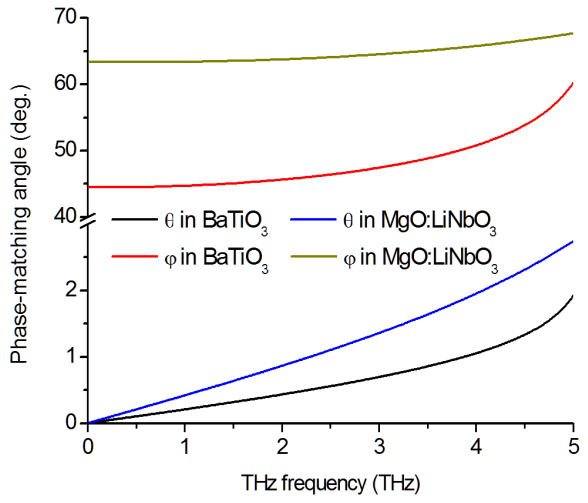

FIG. 3. Relation between THz frequency and the PM angles θ and φ in $BaTiO_3$ and $MgO:LiNbO_3$, for a pump wavelength of 1064 nm.

The PM angles involved in the process of SPS will also vary with the THz frequency. Figure 3 shows the relation between the THz frequency and the PM angles θ and φ, in $BaTiO_3$ and $MgO:LiNbO_3$, with a pump wavelength of 1064 nm. When the frequency varies from 0 to 5 THz, θ varies from 0° to 1.9° in $BaTiO_3$ and from 0° to 2.8° in $MgO:LiNbO_3$, and φ varies from 44.5° to 60.3° in $BaTiO_3$ and from 63.4° to 67.7° in $MgO:LiNbO_3$. Compared to $MgO:LiNbO_3$, the PM angles θ and φ in $BaTiO_3$ are smaller, which means that the NPM configuration in $BaTiO_3$ can provide a larger effective interaction volume among the three mixing waves.

IV. EFFECTIVE PARAMETRIC GAIN LENGTH

The PM angles θ and φ determine the magnitude of the effective parametric gain length of the Stokes and THz waves. Next we deduce the formula for the effective parametric gain length under the NPM condition, based on the theoretical model proposed in Ref. [24]. As shown in Fig. 3, the angle θ in the range of 0°-1.9° in $BaTiO_3$ is equivalent to a double-refraction walk-off angle in Ref. [24], since the magnitudes of both angles are approximately equal, and the effects of both are identical. Assuming that the pump, Stokes, and THz waves have Gaussian profiles, the transverse dimension of the Stokes is simultaneously narrowed by gain polarization and broadened by diffraction. The relation between the pump-wave radius w_p and the Stokes-wave radius w_s is given by

$$\left(\frac{\pi}{2L\lambda_s}\right)^2\left(\frac{w_p^2 w_s^2}{w_p^2+2w_s^2}\right)^3+\frac{w_p^2 w_s^2}{w_p^2+2w_s^2}-\frac{w_p^2}{2}=0 \tag{1}$$

where λ_s is the wavelength of the Stokes wave and L is the optical cavity length, $L = L' + (n_s - 1)l$, n_s is the refractive index of the Stokes wave, L' is the physical length of the Stokes cavity and l is the crystal length. The walk-off length l_ω is given by

$$l_\omega = \frac{\sqrt{\pi}}{2}\frac{w_p}{\theta}\sqrt{\frac{w_p^2+w_s^2}{w_p^2+w_s^2/2}} \tag{2}$$

The effective parametric gain length of the Stokes wave $L_{\text{eff-Stokes}}$ is given by

$$L_{\text{eff-Stokes}} = l_\omega erf\left(\frac{\sqrt{\pi}}{2}\frac{l}{l_\omega}\right) \tag{3}$$

The relationship between the effective parametric gain length of the Stokes wave $L_{\text{eff-Stokes}}$ and that of the THz wave $L_{\text{eff-THz}}$ is given by

$$L_{\text{eff-THz}} = L_{\text{eff-Stokes}} \frac{\sin\theta}{\sin\varphi} \tag{4}$$

The effective parametric gain lengths $L_{\text{eff-Stokes}}$ and $L_{\text{eff-THz}}$ versus pump-wave radius w_p for THz frequencies of 1, 3, and 5 THz are shown in Fig. 4. The effective parametric gain lengths $L_{\text{eff-Stokes}}$ and $L_{\text{eff-THz}}$ monotonically increase with increasing pump-wave radius w_p. The maximum value of $L_{\text{eff-THz}}$ is about 2 mm, and that of $L_{\text{eff-Stokes}}$ is about 59.5 mm. The effective parametric gain lengths $L_{\text{eff-Stokes}}$ and $L_{\text{eff-THz}}$ rapidly increase when the pump wave radius w_p is in the range of 0~0.5 mm, and gradually increase when the pump wave radius w_p is in the range of 0.5~2 mm. When w_p is larger than 2 mm, $L_{\text{eff-Stokes}}$ and $L_{\text{eff-THz}}$ increase slowly. A pump wave with a larger radius can generate a Stokes wave and a THz wave with a large beam radius simultaneously, resulting in a long effective parametric gain length. Actually, for maximum conversion efficiency the pump beam's diameter must be increased until the effective parametric gain length equals the crystal length.

The effective parametric gain lengths $L_{\text{eff-Stokes}}$ and $L_{\text{eff-THz}}$ versus the THz frequency for pump wavelengths of 532, 1550, and 3000 nm are shown in Fig. 5. The effective parametric gain length $L_{\text{eff-Stokes}}$ monotonically decreases with increasing THz frequency. The separation between

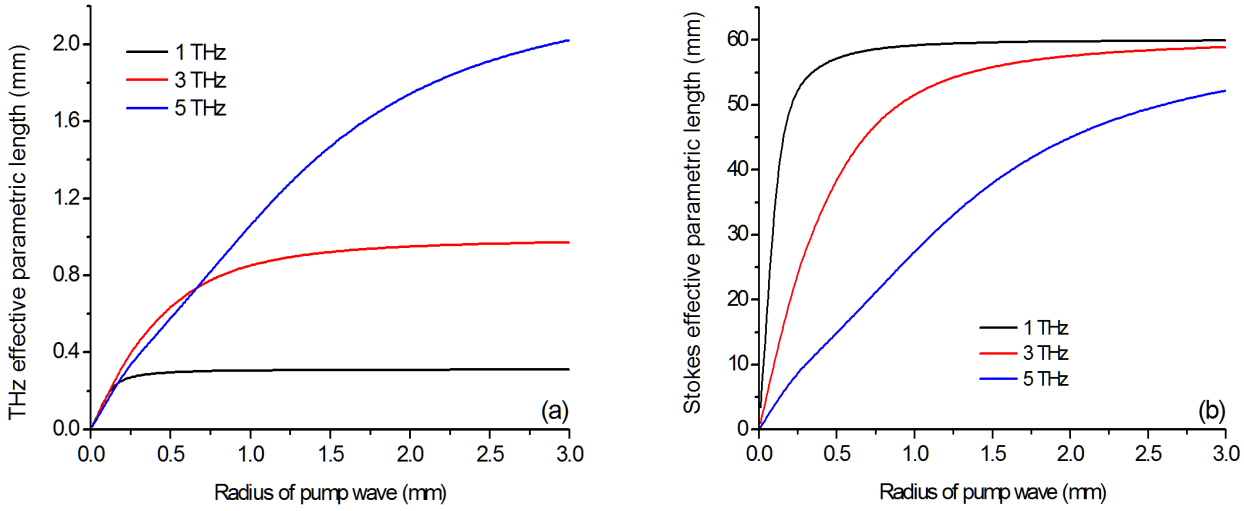

FIG. 4. The effective parametric gain length of the Stokes wave $L_{\text{eff-Stokes}}$ and of the THz wave $L_{\text{eff-THz}}$ versus pump-wave radius w_p, for frequencies of 1, 3, and 5 THz, assuming $l = 60$ mm, and $\lambda_p = 1064$ nm: (a) effective parametric gain length $L_{\text{eff-THz}}$, (b) effective parametric gain length $L_{\text{eff-Stokes}}$.

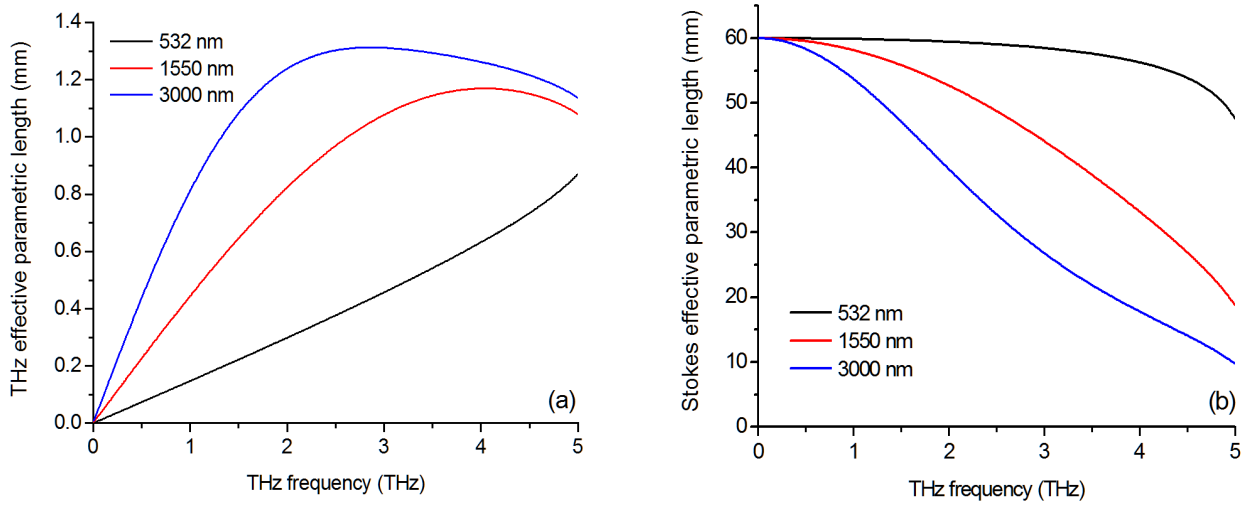

FIG. 5. The effective parametric gain length of the Stokes wave $L_{\text{eff-Stokes}}$ and of the THz wave $L_{\text{eff-THz}}$ versus THz frequency, for the pump wavelengths of 532, 1550, and 3000 nm, assuming $l = 60$ mm, $L' = 1.2l$, and $w_p = 1$ mm: (a) effective parametric gain length $L_{\text{eff-THz}}$, (b) effective parametric gain length $L_{\text{eff-Stokes}}$.

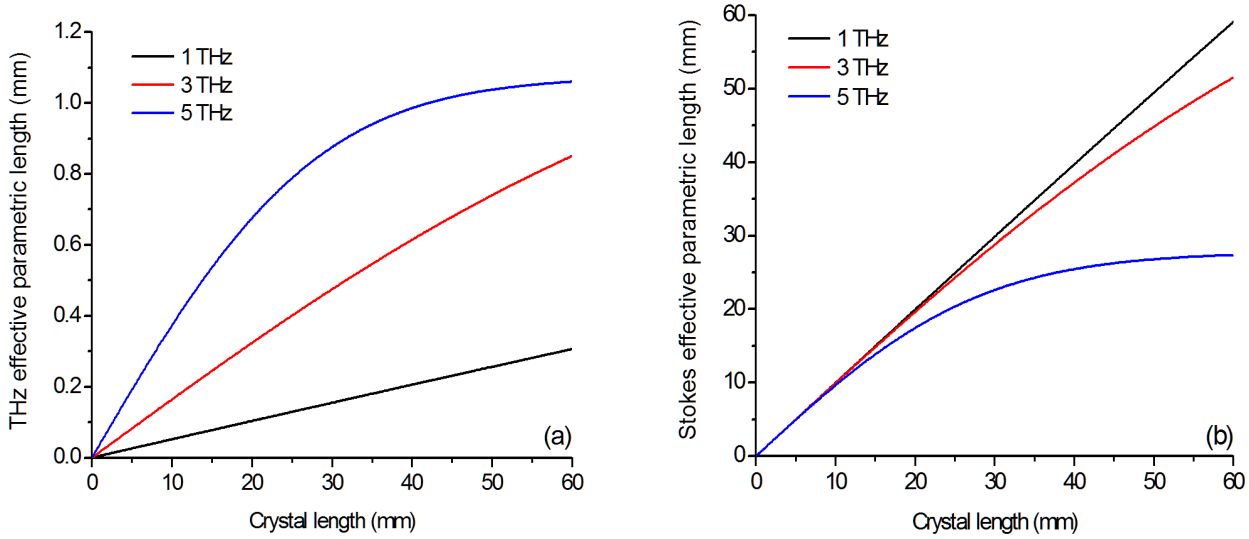

FIG. 6. The effective parametric gain length of the Stokes wave $L_{\text{eff-Stokes}}$ and of the THz wave $L_{\text{eff-THz}}$ versus crystal length l, for frequencies of 1, 3, and 5 THz, assuming $L = 1.2l$, and $w_{\text{p}} = 1$ mm, and $\lambda_{\text{p}} = 1064$ nm: (a) effective parametric gain length $L_{\text{eff-THz}}$, (b) effective parametric gain length $L_{\text{eff-Stokes}}$.

pump and Stokes waves enlarges as the PM angle θ increases with increasing THz frequency. The increase of θ induces the decrease of $L_{\text{eff-Stokes}}$. From Eq. (4) and Fig. 3, the effective parametric gain length $L_{\text{eff-THz}}$ relates to $L_{\text{eff-Stokes}}$, the angle θ, and the angle φ. With increasing THz frequency, the angles θ and φ increase and the $L_{\text{eff-Stokes}}$ decreases, so $L_{\text{eff-THz}}$ does not vary monotonically.

The effective parametric gain length $L_{\text{eff-Stokes}}$ and $L_{\text{eff-THz}}$ versus crystal length l for THz frequencies of 1, 3, and 5 THz are shown in Fig. 6. The effective parametric gain lengths $L_{\text{eff-Stokes}}$ and $L_{\text{eff-THz}}$ monotically enlarge with increasing crystal length l. $L_{\text{eff-Stokes}}$ increases rapidly with crystal length l for the frequencies is 1 and 3 THz, and increases smoothly for a frequency of 5 THz. At lower frequencies of the THz wave, the pump and Stokes waves almost overlap as the PM θ is small. On the contrary, the pump and Stokes waves separate rapidly as the two beams partially overlap at higher THz frequencies.

V. PARAMETRIC GAIN AND ABSORPTION

For high-power THz wave generation, the magnitude of the parametric gain coefficient is important. We calculate the frequency dependence of THz-wave parametric gain g_{T} using the theoretical model proposed by Sussman [8, 25]. The analytic expression for g_{T} under the NPM condition in SI units can be written as [26]

$$g_{\text{T}} = \frac{(\alpha_{\text{T}} + \alpha_{\text{pr}})}{2}\left\{\left[1 + 16\cos\varphi\left(\frac{g_0}{\alpha_{\text{T}} + \alpha_{\text{pr}}}\right)^2\right]^{\frac{1}{2}} - 1\right\} \tag{5}$$

$$g_0^2 = \frac{\omega_{\text{s}}\omega_{\text{T}}}{128\pi^2\varepsilon_0 c^3 n_{\text{p}} n_{\text{s}} n_{\text{T}}} I_{\text{p}}\left(d_E + \sum_j \frac{S_j \omega_{0_j}^2 d_{Q_j}}{\omega_{0_j}^2 - \omega_{\text{T}}^2}\right)^2 \tag{6}$$

$$\alpha_{\text{T}} = 2\frac{\omega_{\text{T}}}{c}\,\text{Im}\left(\varepsilon_\infty + \sum_j \frac{S_j \omega_{0_j}^2}{\omega_{0_j}^2 - \omega_{\text{T}}^2 - i\omega_{\text{T}}\Gamma_j}\right)^{\frac{1}{2}} \tag{7}$$

$$\alpha_{\text{pr}} = \frac{\sin\varphi}{a w_{\text{p}}} \tag{8}$$

where ω_{0_j}, S_j, and Γ_j respectively denote eigenfrequency, oscillator strength of the polariton modes, and the bandwidth of the *jth* A_1-symmetry phonon mode in the $BaTiO_3$ crystal. I_{p} is the power density of the pump wave, g_0 is the low-loss parametric gain, and n_{p} and n_{T} are the refractive indices of the pump and THz waves, respectively. α_{T} is the material absorption coefficient in the THz region, while α_{pr} is the effective absorption coefficient arising from the propagation of the THz wave out of the interaction region among the pump, Stokes, and THz waves, as proposed by Schwarz and Maier [27]. a is a parameter that determines the ratio of the effective diameter of the interaction region to the pump radius w_{p}, and was estimated to be 0.2 [27]. $d_E = 16\pi d_{15}$ and d_Q are nonlinear coefficients related to pure parametric (second-order) and Raman (third-order) scattering processes, respectively.

When the THz frequency is far below that of the lowest TO mode of 178 cm^{-1}, Eq. (6) can be rewritten as [8]

$$g_0^2 = \frac{\omega_{\text{s}}\omega_{\text{T}}}{128\pi^2\varepsilon_0 c^3 n_{\text{p}} n_{\text{s}} n_{\text{T}}} I_{\text{p}}\left(d_E + \sum_j S_j d_{Q_j}\right)^2 \tag{9}$$

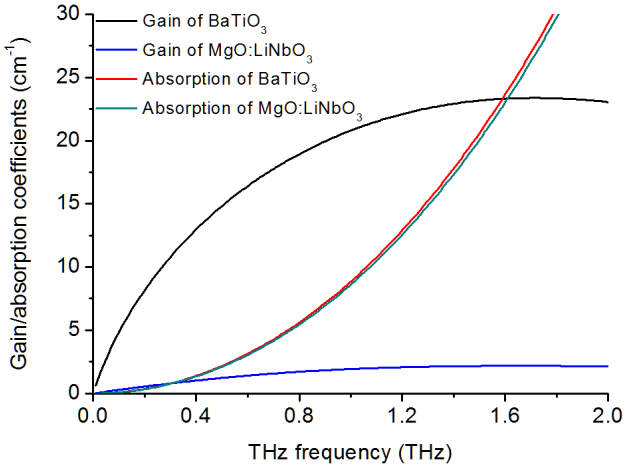

FIG. 7. THz-wave parametric gain coefficients g_T and absorption coefficients α_T for $BaTiO_3$ and $MgO:LiNbO_3$ at room temperature; $\lambda_p = 546.1$ nm, $w_p = 2$ mm, $I_p = 100$ MW/cm^2.

The relationship between d_E and d_Q is given by [8, 28, 29]

$$d_E + \sum_j S_j d_{Q_j} = \frac{1}{4} r_{51} n_p^4 \tag{10}$$

where r_{51} is the linear electro-optic coefficient of $BaTiO_3$. r_{51} is 1640 pm/V at 546.1 nm in unclamped $BaTiO_3$ [30].

According to Eqs. (5)~(10), we plot the values of the THz wave parametric gain coefficient g_T and the absorption coefficient α_T in $BaTiO_3$ and $MgO:LiNbO_3$ in the range of 0~2 THz, at a pump intensity of 100 MW/cm^2, as shown in Fig. 7. In this Letter, the data for $MgO:LiNbO_3$ are taken from Ref. [8]. From the figure we find that the THz absorption coefficients α_T of $BaTiO_3$ and $MgO:LiNbO_3$ are approximately equal, whereas the gain coefficient g_T of $BaTiO_3$ is much larger than that of $MgO:LiNbO_3$. Below 1.0 THz, g_T in $BaTiO_3$ increases rapidly with frequency, while in the range of 1.0~2.0 THz, it varies slowly. The maximum value of g_T in $BaTiO_3$ is 23.4 cm^{-1} at 1.7 THz. The large gain coefficient g_T in $BaTiO_3$ is derived from the third-order nonlinearity d_Q, which originates from ionic polarization. From Eq. (9) we find that g_0 is proportional to the pump intensity I_p. A pump wave with a picosecond or femtosecond pulse width, providing a pump intensity on the order of GW/cm^2, can enlarge the gain coefficient g_T by several orders of magnitude [31-33]. A recent experimental study of $MgO:LiNbO_3$ has shown that the conversion efficiency of a THz wave via SPS can be improved by three orders of magnitude through the use of subnanosecond pump pulses [34].

VI. THZ PHOTON FLUX DENSITY

The coupled wave equations for THz-wave parametric mixing with THz-wave absorption can be found in Ref. [8]. The coupled wave equations describe the field-envelope variation of the pump, Stokes, and THz waves. With strong THz-wave absorption, and without phase mismatch or pump depletion, the coupled wave equations can be solved to give the THz-photon flux density ϕ_T, with a general solution [35] given by

$$\phi_T = \phi_S(0) e^{-(\alpha_T + \alpha_{pr}) L_{eff\text{-}THz}/2} \frac{g_T^2}{g_T^2 + \left(\frac{\alpha_T + \alpha_{pr}}{4}\right)^2} \times \left| \sinh\left(\sqrt{g_T^2 + \left(\frac{\alpha_T + \alpha_{pr}}{4}\right)^2}\, L_{eff\text{-}THz} \right) \right|^2 \tag{11}$$

where the initial THz-photon flux density is assumed to be zero, and $\phi_S(0)$ is the initial Stokes-photon flux density. According to Eq. (11), we plot the THz-photon flux density normalized to the initial Stokes-photon flux density $\phi_T/\phi_S(0)$ for a pump wavelength of 546.1 nm, as shown in Fig. 8. $\phi_T/\phi_S(0)$ monotonically rises with increasing

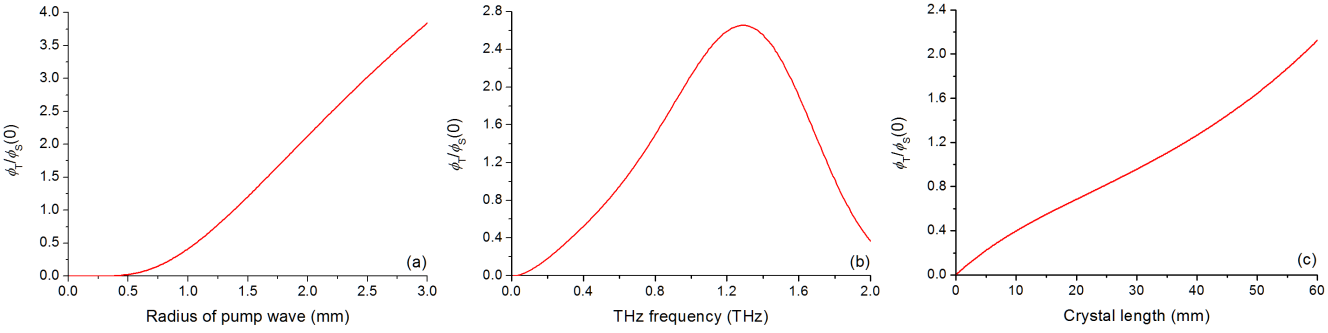

FIG. 8. THz-photon flux density normalized to the initial Stokes-photon flux density $\phi_T/\phi_S(0)$, for pump wavelength of 546.1 nm and pump intensity of 100 MW/cm^2: $\phi_T/\phi_S(0)$ versus radius of the pump wave at 1 THz, assuming $l = 60$ mm and $L' = 1.2l$; (b) $\phi_T/\phi_S(0)$ versus THz frequency, assuming $l = 60$ mm, $L' = 1.2l$, and $w_p = 2$ mm; (c) $\phi_T/\phi_S(0)$ versus crystal length at 1 THz, assuming $L' = 1.2l$, $w_p = 2$ mm.

pump-wave radius w_p, as shown in Fig. 8(a). The monotonic increase of the effective parametric gain length $L_{\text{eff-THz}}$ with increasing pump-wave radius w_p, as shown in Fig. 4, leads to the monotonic increase of $\phi_T/\phi_S(0)$. $\phi_T/\phi_S(0)$ slowly increases when w_p is in the range of 0~0.5 mm, then rapidly increases when w_p is larger than 0.5 mm. The maximum value of $\phi_T/\phi_S(0)$ is 3.84. It should be noted that in the calculations we assume the pump intensity is invariant when the pump-wave radius is varying; in fact, the pump intensity decreases with the increase in pump-wave radius, which decreases the parametric gain. For this reason, the rate of increase of $\phi_T/\phi_S(0)$ with the increase of pump-wave radius slows. Figure 8(b) shows the relation between $\phi_T/\phi_S(0)$ and THz-wave frequency. $\phi_T/\phi_S(0)$ increases in the range of 0~1.29 THz and decreases in the range of 1.29~2 THz, with a maximum value of $\phi_T/\phi_S(0)$ 2.65 at 1.29 THz. Figure 8(c) shows the relation between $\phi_T/\phi_S(0)$ and crystal length l. $\phi_T/\phi_S(0)$ monotonically rises with the increase of crystal length l. The maximum value of $\phi_T/\phi_S(0)$ is 2.13. $L_{\text{eff-THz}}$ increases rapidly with increasing crystal length l, as shown in Fig. (6), which leads to the enhancement of THz-photon flux density along with crystal length l. From Fig. 8, the value of $\phi_T/\phi_S(0)$ can be enhanced by selecting proper parameter values, so it is possible to generate a high-power THz wave by injecting a Stokes seed wave [34].

THz wave generation via SPS in $BaTiO_3$ bulk crystal has certain advantages over that in bulk MgO:$LiNbO_3$. First, the PM angles θ and φ in $BaTiO_3$ are smaller than those in MgO:$LiNbO_3$, indicating that the NPM configuration in $BaTiO_3$ can provide larger effective interaction volume among the three mixing waves and longer effective parametric gain length. Second, the effective parametric gain coefficients in $BaTiO_3$ are much larger than those in MgO:$LiNbO_3$.

VII. CONCLUSION

SPS from the A_1 TO modes of $BaTiO_3$ bulk crystal under the NPM condition can efficiently generate a THz wave. The PM angles in $BaTiO_3$ are smaller than those in MgO:$LiNbO_3$. The effective parametric gain length of the Stokes and THz waves relate to the radius of the pump wave, the THz frequency, and the crystal length. The effective parametric gain coefficients in $BaTiO_3$ are much larger than those in MgO:$LiNbO_3$. Larger radius of the pump wave and longer crystal length can generate a THz wave with a larger phonon flux density. The high gain coefficients and large interaction volume among the three mixing waves indicate that $BaTiO_3$ is an attractive optical crystal for THz wave generation via SPS.

ACKNOWLEDGMENT

This study was supported by the National Natural Science Foundation of China (61601183); Natural Science Foundation of Henan Province (162300410190); Program for Innovative Talents (in Science and Technology) in University of Henan Province (18HASTIT023); Young Backbone Teachers in University of Henan Province (2014GGJS-065); and the Program for Innovative Research Team (in Science and Technology) in University of Henan Province (16IRTSTHN017).

REFERENCES

1. K. Kawase, J. Shikata, and H. Ito, "Terahertz wave parametric source," J. Phys D: Appl. Phys. **35**, R1-R14 (2002).
2. T. Ikari, X. Zhang, H. Minamide, and H. Ito, "THz-wave parametric oscillator with a surface-emitted configuration," Opt. Express **14**, 1604-1610 (2006).
3. T. A. Ortega, H. M. Pask, D. J. Spence, and A. J. Lee, "THz polariton laser using an intracavity Mg:$LiNbO_3$ crystal with protective Teflon coating," Opt. Express **25**, 3991-3999 (2017).
4. R. Zhang, Y. Qu, W. Zhao, and Z. Chen, "High energy, widely tunable Si-prism-array coupled terahertz-wave parametric oscillator with a deformed pump and optimal crystal location for angle tuning," Appl. Opt. 56, 2412-2417 (2017).
5. Y. Wang, L. Tang, D. Xu, C. Yan, Y. He, J. Shi, D. Yan, H. Liu, M. Nie, J. Feng, and J. Yao, "Energy scaling and extended tunability of terahertz wave parametric oscillator with MgO-doped near-stoichiometric $LiNbO_3$ crystal," Opt. Express **25**, 8926-8936 (2017).
6. H. Jang, G. Strömqvist, V. Pasiskevicius, and C. Canalias, "Control of forward stimulated polariton scattering in periodically-poled KTP crystals," Opt. Express **21**, 27277-27283 (2013).
7. H. Jang, A. Viotti, G. Strömqvist, A. Zukauskas, C. Canalias, and V. Pasiskevicius, "Counter-propagating parametric interaction with phonon-polaritons in periodically poled $KTiOPO_4$," Opt. Express **25**, 2677-2686 (2017).
8. S. S. Sussman, "Tunable light scattering from transverse optical modes in lithium niobate," Stanford University, Stanford, California, Microwave Laboratory Report No. 1851 (1970).
9. W. Wang, Z. Cong, X. Chen, X. Zhang, Z. Qin, G. Tang, N. Li, C. Wang, and Q. Lu, "Terahertz parametric oscillator based on $KTiOPO_4$ crystal," Opt. Lett. **39**, 3706-3709 (2014).
10. W. Wang, Z. Cong, Z. Liu, X. Zhang, Z. Qin, G. Tang, N. Li, Y. Zhang, and Q. Lu, "THz-wave generation via stimulated polariton scattering in $KTiOAsO_4$ crystal," Opt. Express **22**, 17092-17098 (2014).
11. A. J. Lee and H. M. Pask, "Continuous wave, frequency-tunable terahertz laser radiation generated via stimulated polariton scattering," Opt. Lett. **39**, 442-445 (2014).
12. T. A. Ortega, H. M. Pask, D. J. Spence, and A. J. Lee, "Stimulated polariton scattering in an intracavity $RbTiOPO_4$ crystal generating frequency-tunable THz output," Opt. Express **24**, 10254-10264 (2016).

13. T. D. Wang, Y. C. Huang, M. Y. Chuang, Y. H. Lin, C. H. Lee, Y. Y. Lin, F. Y. Lin, and G. Kh. Kitaeva, "Long range parametric amplification of THz wave with absorption loss exceeding parametric gain," Opt. Express **21**, 2452-2462 (2013).
14. J. A. Sanjurjo, R. S. Katiyar, and S. P. S. Porto, "Temperature dependence of dipolar modes in ferroeiectric $BaTiO_3$ by infrared studies," Phys. Rev. B **22**, 2396-2403 (1980).
15. A. Pinczuk, W. Taylor, and E. Burstein, "The Raman spectrum of $BaTiO_3$," Solid State Commun. **5**, 429-433 (1967).
16. A. Scalabrin, A. S. Chaves, D. S. Shim, and S. P. S. Porto, "Temperature dependence of the A_1 and E optical phonons in $BaTiO_3$," Phys. Stat. Sol. (b) **79**, 731-742 (1977).
17. D. E. Zelmon, D. L. Small, and P. Schunemann, "Refractive index measurements of barium titanate from .4 to 5.0 microns and implications for periodically poled frequency conversion devices," MRS Online Proc. Libr. **484**, 537-541 (1997).
18. D. N. Nikogosyan, Nonlinear optical crystals: a complete survey, Springer Science & Business Media, 2006.
19. T. F. Boggess, J. O. White, and G. C. Valley, "Two-photon absorption and anisotropic transient energy transfer in $BaTiO_3$ with 1-psec excitation," J. Opt. Soc. Am. B **7**, 2255-2258 (1990).
20. G. A. Brost, R. A. Motes, and J. R. Rotge, "Intensity-dependent absorption and photorefractive effects in barium titanate," J. Opt. Soc. Am. B **5**, 1879-1885 (1988).
21. J. B. Khurgin, D. Yang, and Y. J. Ding, "Generation of mid-infrared radiation in the highly-absorbing nonlinear medium," J. Opt. Soc. Am. B **18**, 340-343 (2001).
22. Y. J. Ding, "Efficient generation of high-frequency terahertz waves from highly lossy second-order nonlinear medium at polariton resonance under transverse-pumping geometry," Opt. Lett. **35**, 262-264 (2010).
23. Y. J. Ding, "Efficient generation of far-infrared radiation from a periodically poled $LiNbO_3$ waveguide based on surface-emitting geometry," J. Opt. Soc. Am. B **28**, 977-981 (2011).
24. S. J. Brosnan and R. L. Byer, "Optical parametric oscillator threshold and linewidth studies," IEEE J. Quantum Electron. **15**, 415-431 (1979).
25. Y. Takida, J. Shikata, K. Nawata, Y. Tokizane, Z. Han, M. Koyama, T. Notake, S. Hayashi, and H. Minamide, "Terahertz-wave parametric gain of stimulated polariton scattering," Phys. Rev. A **93**, 043836 (2016).
26. D. A. Walsh, *Intracavity terahertz optical parametric oscillators* (Doctoral dissertation, University of St Andrews, 2011).
27. U. T. Schwarz and M. Maier, "Damping mechanisms of phonon polaritons, exploited by stimulated Raman gain measurements," Phys. Rev. B **58**, 766-775 (1998).
28. A. Yariv, *Quantum Electronics, 3rd ed.* (Wiley, 1988), Chapter 16.
29. W. D. Johnston and I. P. Kaminow, "Contributions to optical nonlinearity in GaAs as determined from Raman scattering efficiencies," Phys. Rev. **188**, 1209-1211 (1969).
30. A. R. Johnston and J. M. Weingart, "Determination of the low-frequency linear electro-optic effect in tetragonal $BaTiO_3$," J. Opt. Soc. Am. **55**, 828-834 (1965).
31. W. Shi, Y. J. Ding, N. Fernelius, and K. L. Vodopyanov, "An efficient, tunable, and coherent 0.18-5.27 THz source based on GaSe crystal," Opt. Lett. **27**, 1454-1456 (2002).
32. Y. J. Ding, "Efficient generation of high-Power quasi-single-cycle THz pulses from single infrared beam in second-order nonlinear medium," Opt. Lett. **29**, 2650-2652 (2004).
33. Y. J. Ding, "Quasi-single-cycle THz pulses based on broadband-phase-matched difference-frequency generation in second-order nonlinear medium: High output powers and conversion efficiencies," IEEE J. Sel. Top. Quantum Electron. **10**, 1171-1179 (2004).
34. S. Hayashi, K. Nawata, T. Taira, J. Shikata, K. Kawase, and H. Minamide, "Ultrabright continuously tunable terahertz-wave generation at room temperature," Sci. Rep. **4**, 5045 (2014).
35. G. Kh. Kitaeva and A. N. Penin, "Parametric frequency conversion in layered nonlinear media," J. Exp. Theor. Phys. **98**, 272-286 (2004).